EGFR activation correlates with intracranial pressure and outcome in a mixed intracranial bleeding porcine model

Zongren Zhao[1], Andrea Hoffmann[2], Michael Gröger[2], Sandra Kress[2], Franziska Münz[3], Fan Sun[1], Tamara Merz[2,3], Magnus Scheer[4], Enrico Calzia[2], Burak Özkan[1], Peter Radermacher[2,5], Francesco Roselli[1,6], *Thomas Kapapa[7], *Marica Pagliarini[1]

Affiliations:
1. Dept. of Neurology, Ulm University, 89081 Ulm,
2. Institute of Anaesthesiological Pathophysiology and Process Development, University Hospital Ulm, 89081 Ulm, Germany
3. Dept. of Anesthesia and Intensive Care, Ulm University Medical Center, Ulm, Germany
4. Dept. of Neurosurgery, German Armed Forces Hospital Ulm, Ulm, Germany
5. Dept. of Intensive Care Medicine, Angers University Hospital, Angers, France
6. German Center for Neurodegenerative Diseases (DZNE)-Ulm, 89081 Ulm Germany
7. Dept. of Neurosurgery, University Hospital Ulm, 89081 Ulm, Germany

*Co-Senior Authors

Corresponding author: Marica Pagliarini, PhD
Dept. of Neurology, Ulm University
Center for Biomedical Research
Helmholtzstrasse 8/1 89081 Ulm DE
Phone: 0049 0731 65153
e-mail: marica.pagliarini@uni-ulm.de

Abstract

The pig model is an advanced system for studying human brain injury due to its anatomical similarities with the brain, such as brain size, gyrencephalic structure, skull shape, and white-to-gray matter ratio. Brain hemorrhage increases intracranial pressure through blood accumulation and brain swelling, leading to impaired cerebral blood flow, ischemia, and potentially, secondary injury, thus further exacerbating neurological damage. This study investigates the role of receptor tyrosine kinases (RTKs) in the injury response and clinical outcomes, focusing on their potential as therapeutic targets for intracranial pressure control after injury.

To this end, we developed a sustained, resuscitated pig model of acute mixed intracranial bleeding with ICP and hemorrhagic shock. Multimodal brain monitoring and neurological assessments offered insights into the progression of the injury.

Our findings showed that 36-48 hours post-injury, animals exhibited signs of cerebral tissue hypoxia, neuroinflammation, and extensive tissue damage. Elevated HIF1-α expression in the injured hemisphere confirmed local hypoperfusion. Inflammatory markers such as TNF-α, CD68, and MMP-9 were upregulated in both hemispheres, reflecting a generalized neuroinflammatory response. Gene expression analysis revealed increased markers of vascular, astrocytic, and neuroimmune activation, particularly related to endothelial integrity and astrocyte activation.

RTK expression analysis showed increased levels of VEGFR1, VEGFR2, Tie-2, EGFR, and Axl in the injured cortex, with activation of EGFR/ErbB4 and HGFR/Met pathways. Hierarchical clustering of our transcriptional analysis revealed distinct patterns of activation, highlighting the direct relationship between severity of ICP increase and astrocyte response. In particular, EGFR phosphorylation correlated with i) severity of ICP increase, ii) neurological evaluation using a modified Glasgow Coma Scale, and iii) survival.

These findings suggest that modulating EGFR signaling may offer a therapeutic approach for managing ICP and improving outcome in traumatic brain injury.

Introduction

Increased intracranial pressure (IntraCranial Hypertension, ICH) frequently occurs in severe Traumatic Brain Injury (TBI) [1] as well as in acute cerebrovascular conditions (subdural haematoma - SH- , intraparenchymal haemorrhage –IH) [2]. ICH constitutes an independent prognostic factor, with high levels of intracranial pressure (ICP) or prolonged elevations in ICP corresponding to less favorable prognosis both in TBI [3] and in IH [4] due to cerebral ischemia, brainstem compression and herniation. Treatment is limited to the use of analgetics and sedatives, [5] hyperosmotic solutions, [6] short-term hyperventilation, [7] and, ultimately, surgical decompression by craniectomy. [8]

The pathophysiology of increased ICP after vascular/traumatic brain injury not only involves the cytotoxic component associated with ischemia[9], but also a number of active processes directed to the control of water and electrolyte fluxes in and out of the neurovascular unit and of the brain parenchyma through the neurovascular and lymphatic interfaces [10,11]. At the level of the neurovascular unit, the vasogenic brain edema (VBE) is thought to be associated with the increased permeability of the blood-brain-barrier due to endothelial activation driven by the abundance of vascular permeability modulators (including growth factors, cytokines and proteases such as MMP9[12,13], and by endothelial dysfunction associated with hypoxia and ischemia[14]. Furthermore, impaired water drainage through astrocytes[10,15] contributes to the establishment of brain edema.

Interference with these processes is necessary to deliver therapeutic interventions that can reduce VBE and lower ICP, thus addressing ICH at a mechanistic level. Members of the Receptor Tyrosine Kinases family (RTK) display several characteristics that make them suitable entry-points for this aim: several RTKs can deeply influence the cell biology of endothelial cells (such as VEGFR and Tie2[13,16], astrocytes (EGFR, FGFR[17], and inflammatory subpopulations (such as Met, Axl, FGFR[18,19]; RTK have discrete spatio-temporal patterns of phosphorylation after brain injury[18,19] and, importantly, are already targeted by a number of selective inhibitors, thus being amenable to drug repurposing [20].

In order to point out the translational potential of RTK inhibitors as treatment agents for brain edema and, consequently, of intracranial hypertension, in TBI and ICH, it is first necessary to map the temporal pattern of RTK expression and activation over the physiological readouts relevant for neurocritical care, such as ICP. Here we have adopted a porcine Mixed-IntraCranial Bleeding model (pMICB[21]) to link RTKs activation to the pathophysiology of brain edema and intracranial hypertension.

Material and methods

Animal model and surgery

All experiments were conducted in strict adherence to the National Institutes of Health (NIH) Guidelines on the Use of Laboratory Animals and the European Union's Directive 2010/63/EU regarding the protection of animals used for scientific purposes. Approval was obtained from the local Animal Care Committee and the Federal Authorities for Animal Research (Regierungspräsidium Tübingen; Reg.-Nr. 1559, approval 29 October 2021). Premedication consisted of intramuscular azaperone (5 mg/kg) and midazolam (1–2 mg/kg). After establishing venous access *via* an ear vein, anesthesia was induced with propofol (1–2 mg/kg) and ketamine (1 mg/kg), followed by endotracheal intubation and controlled mechanical ventilation. Ventilation parameters included a tidal volume of 8 mL/kg, respiratory rate of 8–12 breaths/min to maintain a PCO_2 of 35–40 mmHg, inspiration-to-expiration (I/E) ratio of 1:1.5, and a positive end-expiratory pressure (PEEP) of 10 cm H_2O and an F_iO_2 of 0.3. Anesthesia was maintained with continuous intravenous propofol (10 mg/kg/hour), remifentanil (initial bolus 5 µg/kg, followed by 15–20 µg/kg/hour), and midazolam 1 mg/kg/h. Maintenance fluids (10 mL/kg/hour) consisted of a balanced electrolyte solution (Jonosteril 1/1, Fresenius Kabi, Germany).

Both femoral arteries were then accessed to insert a 4-F PiCCO catheter (PULSION Medical Systems) for continuous monitoring of cardiac output, pulse pressure, and stroke volume variation. Additionally, a 10-F catheter was placed for blood sampling and passive blood removal to induce hemorrhagic shock. Subsequently, a 3-lumen catheter was inserted into the left femoral vein for continuous monitoring of blood pressure and cardiac output. Neurosurgical procedures included a midline incision to access the skull, where burr holes (approx. 10 mm) were drilled bilaterally. After dura exposure, a subdural drainage (9-French) was inserted on the left and right side, followed by the placement about 1–1.5 cm subcortical of a multimodal intraparenchymal probe (Neurovent PTO, Raumedic) for monitoring intracranial pressure (ICP), brain temperature (BT), and brain oxygen partial pressure ($P_{bt}O_2$). After the probe was placed, the dura and drill holes were sealed, and the wound was carefully sutured.

After a 60-minute rest period, ventilation parameters were adjusted to F_iO_2 of 0.21, PEEP of 0 cm H_2O, and I/E ratio of 1:2. Thereafter, 0.1 mL/kg of autologous blood were injected into the subdural space *via* the drainage tube over 15 minutes, which was immediately followed by passive removal of blood over 30 minutes targeting 30 % of the calculated blood volume. Blood removal was decelerated or interrupted as necessary to maintain cerebral perfusion pressure (CPP) ≥ 50 mmHg[22,23].

Continuous monitoring was performed throughout the experiment, including heart rate, blood pressure, hemogloblin O_2 saturation, ICP, CPP, $P_{bt}O_2$ and BT. Two hours post-injection, ~~targeted~~ resuscitation was initiated. Resuscitation included retransfusion of shed blood within 30 min, fluid administration (10 mL/kg/h Ionosteril, reduced to 5 mL/kg/h if central venous pressure > 16 mmHg and/or in case of oliguria) as well as by continuous i.v. noradrenaline titrated to the MAP at pre-shock levels (± 10%) and CPP at baseline levels and at least > 60 mmHg. Every 24 hours, anesthetic depth was reduced until adequate spontaneous breathing resumed, and neurological function was assessed using a modified Glasgow Coma Scale for pigs as previously reported[22,24].

Animals were euthanized before the completion of the planned monitoring and treatment period if their CPP dropped below 60 mmHg despite receiving the maximum dose of vasopressors (with a heart rate limit of 160 beats per minute to prevent myocardial injury from tachycardia) and/or if they developed acute anuric kidney failure with hyperkalemia (blood potassium > 6 mmol/l) and cardiac arrhythmias. Naive animals only underwent 3 hours anesthesia without any brain instrumentation.

RNA extraction and qPCR

Cerebral cortex samples were collected from the penumbral region when the hematoma area was visible. The hemisphere with blood injection was defined as "*ipsilateral*" and the opposite hemisphere as "*contralateral*". Tissue sampling was performed in the regions adjacent to the surgical instrumentation sites of both sides.

Tissue samples were homogenized in QIAzol reagent (Qiagen, Cat. No. 79306), and total RNA was extracted following chloroform phase separation and purification using the RNeasy Mini Kit (Qiagen, Cat. No. 74104) according to the manufacturer's protocol, including on-column DNase digestion. RNA was eluted in RNase-free water and stored at −80°C.

Porcine-specific primers were designed using NCBI Primer-BLAST, optimized for 70–140 bp amplicon size and a melting temperature of 60 ± 3°C. Primers were screened for specificity and validated prior to use. Quantitative PCR (qPCR) was performed on the QuantStudio 1 system (ThermoFisher) using SYBR™ Green Universal Master Mix (Applied Biosystems, Cat. No. A46109). Each 10 µL reaction contained 2 µL cDNA, 5 µL Master Mix, and 3 µL primer mix, and all samples were analyzed in duplicate. GAPDH served as the internal control, and relative mRNA expression was calculated using the 2^−ΔCt method.

Protein extraction and Western Blot

Protein concentrations were determined using the BCA Protein Assay Kit (Thermo Fisher Scientific, Cat. No. 23225) according to the manufacturer's instructions. Seventy-five micrograms of protein were mixed with 1× loading buffer, 5% 2-mercaptoethanol, and RIPA buffer, then heated at 95°C for 5 minutes.

Proteins were separated on 8% or 12% SDS-PAGE gels and transferred to PVDF membranes at room temperature for 2 hours. Membranes were blocked in 5% bovine serum albumin (BSA) in 1× Tris-buffered saline with 0.1% Tween-20 (TBST) for 1 hour at room temperature, followed by incubation with primary antibodies overnight at 4°C. After three washes in TBST (10 minutes each), membranes were incubated with appropriate secondary antibodies diluted in 5% BSA/TBST for 2 hours at room temperature, followed by three additional washes.

Proteins were detected using an enhanced chemiluminescence (ECL) system (Bio-Rad, Cat. No. 1705061), and band intensities were quantified using ImageJ software, with normalization to β-actin. Antibody details are provided in Supplementary Table 2.

Porcine Cytokine Antibody Array

Tissue samples were analyzed using the G-Series Porcine Cytokine Array 4 (RayBiotech, Cat. No. GSP-CYT-4-1) according to the manufacturer’s instructions. Tissue lysates were prepared at a total protein concentration of 1 mg/mL, with additional dilution applied to samples exceeding the detection range. Glass slides were equilibrated to room temperature for 20–30 minutes and air-dried for 1–2 hours before blocking for 30 minutes at room temperature.

After removal of the blocking buffer, 100 μL of sample was added to each well and incubated overnight at 4°C. Slides were then washed under gentle shaking at room temperature. A biotinylated antibody cocktail was reconstituted in Sample Diluent, briefly centrifuged, and 80 μL were added per well for a 2-hour incubation at room temperature. Subsequently, Cy5 dye-conjugated streptavidin was prepared and 80 μL were added to each well, followed by 1-hour incubation in the dark at room temperature. Slides were disassembled carefully to avoid contact with the array surface, and fluorescence signals were detected using a laser scanner with a Cy5 detection channel. Raw fluorescence data were extracted using the provided GAL file and analyzed with GenePix microarray analysis software. Data normalization and background correction were performed using the RayBio Analysis Tool to ensure intra- and inter-slide consistency.

Bioinformatic analysis

Cluster analysis was conducted using the K-means algorithm to identify patterns of correlation among molecular markers in scikit-learn module[25] of Python 3.11.6. To visualize the results was used matplotlib [26] The number of clusters ($k = 7$) was determined by evaluating silhouette scores (0.207) across a range of k values and selecting the value that maximized cluster separation while retaining biological interpretability.

To estimate the relative contributions of individual cell types to the gene expression profile of the most prominent cluster, we generated a cell type–specific gene expression signature matrix using single-cell RNA sequencing data annotated with cell types from the Allen Brain Atlas [27] . The dataset was processed using Scanpy[28], and cells were grouped according to the curated cell type labels provided by the Allen Brain reference taxonomy.

For each annotated cell type, we computed the average gene expression across all cells using Scanpy[28], resulting in a signature matrix with genes as rows and cell types as columns. For each gene, the expression value was converted to a 1-10 scale, and the resulting value was expressed as an enrichment score (ES).

After calculating the ES, we evaluated the protein-protein interaction (PPI) using the STRING database (version 11.5)[29]. The input protein list included members of the identified clusters, along with proteins enriched in astrocytes (ES > 4). The STRING analysis was configured with *Sus scrofa* and a minimum required interaction score of 0.4. All interaction evidence sources were enabled. The resulting PPI network was exported to Cytoscape (version 3.10.2)[30]. Degree centrality was calculated using the NetworkAnalyzer plugin to identify hub proteins with the highest number of direct interactions.

Statistical procedures

Normality of the data was tested for all groups using the Shapiro–Wilk test. Pearson's linear correlation coefficient (r) and p-values were calculated for each correlation. Quantitative data are presented as mean ± SD. Group differences were analyzed using an unpaired t-test for normally distributed data, or the Mann-Whitney test for non-normally distributed data. A p-value of <0.05 was considered statistically significant. All statistical analyses were conducted using GraphPad Prism 9.0 (GraphPad Software).

Results

Intracranial hypertension and bilateral cerebral tissue involvement in the porcine mixed-intracerebral bleeding model.

The subdural injection of 0.1mL/kg of autologous blood in correspondence of the parietal lobe (Fig. 1A) not only resulted in the formation of an acute subdural hematoma, but also in the percolation of blood in the sub-arachnoid space and, often, even in the penetration of the brain parenchyma; therefore, we refer to this model as MICB. Despite the inter-individual variability, involvement of the subdural and parenchymal compartments was detected at necropsy in 8/10 animals, with less frequent macroscopic involvement of the sub-arachnoid space ipsi- and controlaterally to the injury hemisphere (Fig. 1B). Soon after the procedure, ICP increased and CPP decreased when compared to previously reported reference ranges[24], confirming the construct validity of the model in both hemispheres (Fig. 1C). Animals (n= 10) were sacrificed between 36 and 48h after the intracranial blood injection, according to above mentioned the termination criteria

We verified the occurrence of hypoxia, neuroinflammation and, more broadly, tissue damage at the endpoint, by a gene expression panel, to provide a quality-control validation of the samples (compared to injury-naive animals, subject to anesthesia but not to neurosurgical instrumentation. Indeed, expression of TNF-α and of the phagocytic markers CD68 and MMP-9 was upregulated both in ipsi- and controlateral tissue samples (Fig. 1D-E), confirming the tissue involvement. On the other hand, expression of the hypoxia-inducible factor 1-alpha (HIF1-α) was upregulated in the ipsilateral hemisphere in the injured animals, but not in the contralateral one, indicating regional hypoperfusion/hypoxia (Fig. 1D-E). Thus, the pMICB results in ICP increase, ipsilateral hypoxia and bilateral neuroinflammation/tissue damage.

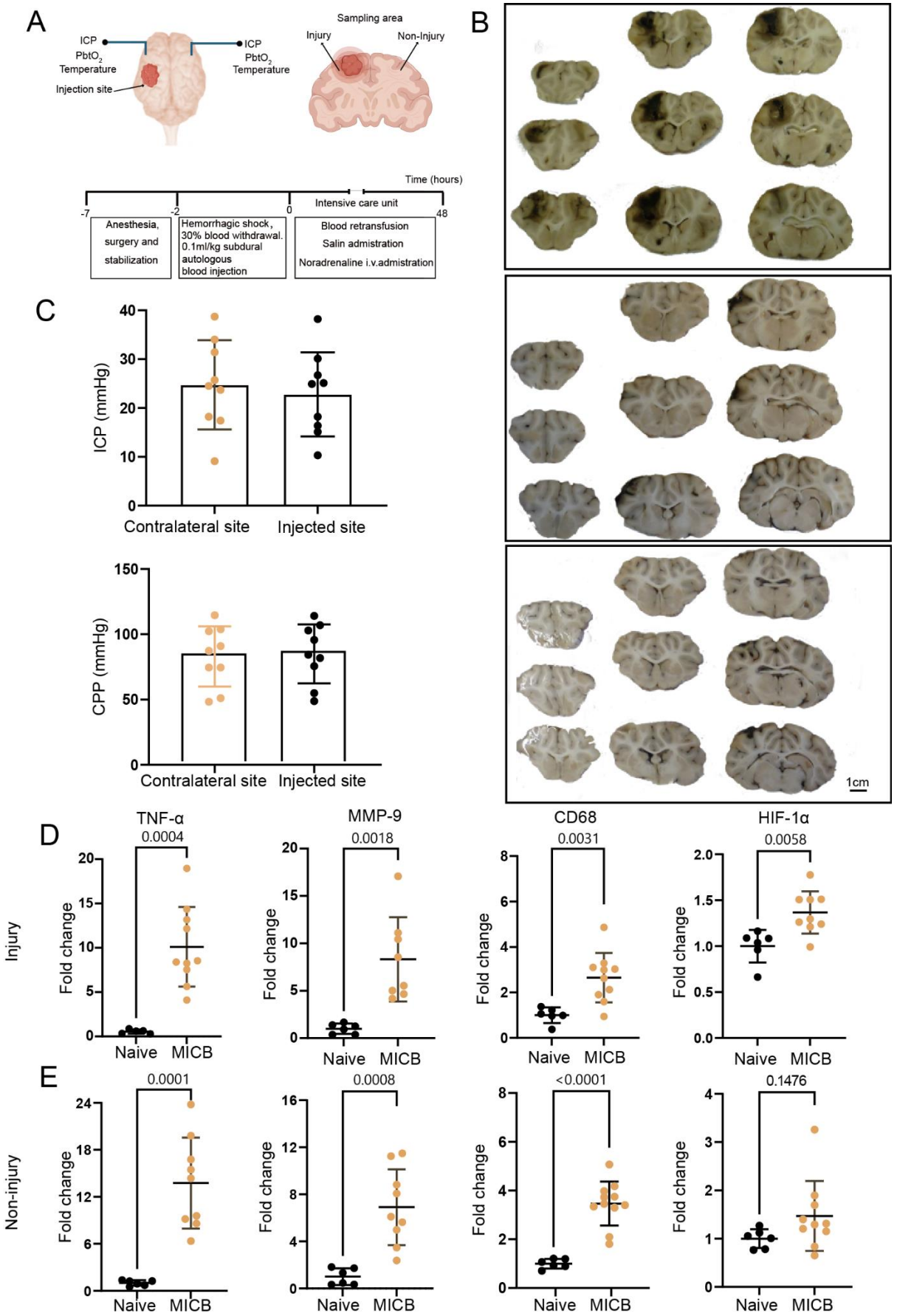
A
ICP
PbtO2
Temperature
Injection site
ICP
PbtO2
Temperature
Sampling area
Injury
Non-Injury
Time (hours)
-7
-2
0
48
Intensive care unit
Anesthesia, surgery and stabilization
Hemorrhagic shock, 30% blood withdrawal. 0.1ml/kg subdural autologous blood injection
Blood retransfusion
Salin admistration
Noradrenaline i.v.admistration
B
1cm
C
ICP (mmHg)
Contralateral site
Injected site
CPP (mmHg)
Contralateral site
Injected site
D
Injury
TNF-α
0.0004
MMP-9
0.0018
CD68
0.0031
HIF-1α
0.0058
Fold change
Naive
MICB
E
Non-injury
0.0001
0.0008
<0.0001
0.1476
Fold change
Naive
MICB

Figure 1. Subdural blood injection results in a porcine mixed-intracranial bleeding model with intracranial hypertension and diffuse cerebral tissue involvement. A. Experimental design. The experimental animals were subjected to anesthesia and (neuro)surgical instrumentation before being subject to the subdural injection of 0.1 mL/kg of autologous blood volume and subsequent hemorrhage. Animals were monitored for up to 48 hours or to the occurrence of termination criteria. B. Macroscopic post-mortem examination of the porcine brains; the patterns of blood diffusion include subdura-intraparenchymal (upper panel), subdural only (middle panel) or sub-arachnoid (lower panel) involvement. C. Physiological measurements at termination display increased ICP values both in the injected and controlateral side, and decreased CPP values in both hemispheres. D. Upregulation of tissue damage markers in cortical tissue from the injury side. Compared to the naive samples, cortical samples from the injected side display upregulation of TNF-α, MMP-9, CD68 and the hypoxia marker HIF1-α. E. Upregulation of injury markers on the controlateral cortical side. Compared to naive samples, cortical tissue from the opposite side of the injection displayed the upregulation of TNF-α, MMP-9, CD68 but no difference in HIF1-α. Scale Bar: 1 cm. naive animals n=6, MICB animals n=10 ; MICB= Mixed IntraCranial Bleeding.

Discrete expression pattern of RTK and RTK ligands in the pMICB

Next, we investigated the extent of vascular, glial and neuroimmune activation ongoing in the porcine brain at the time of sacrifice (36-48h after the injury). We exploited an mRNA expression panel including genes related to endothelial cell and blood-brain-barrier integrity (Claudin-5, VCAM-1, Zonula-Occludens 1 [ZO-1]), to astrocytes reactions (GFAP, AQP4, S100b) and a set of pro- (CCL2, IFN-ɣ, IL-1β) or anti-inflamamtory (IL-10, IL-4, IL-13) immune mediators.

Astrocyte-enriched genes GFAP, AQP4, and S100b were all significantly upregulated in the cortex of the injured side (Fig. 2A). Claudin-5 and VCAM-1, endothelial-barrier integrity markers, were also significantly upregulated (ZO-1 showed no change; Fig. 2B). Likewise, both pro- and anti-inflammatory mediators were consistently elevated (Fig. 2C).

Having established the reactivity of astrocytes, endothelial cells and immune cells in the pMICB samples, we sought to identify RTKs that could be associated to these cellular responses. We first considered a subset of RTK (18/58, prioritized depending on their biological function and translational potential) including RTK involved in vascular permeability

(VEGFR1, VEGFR2, Tie-2; [31-33] , astrocyte proliferation (EGFR, PDGFRa; [34,35]), inflammatory responses (HGFR, MerTK, Axl; [18,36]). Compared to samples from naive animals, injured tissue samples displayed a significant upregulation in the expression of multiple RTKs (Fig. 2D) including VEGFR1, VEGFR2, Tie-2, IGF-1, EGFR, ErbB4 and FGFR1, as well as the inflammation-related HGFR and Axl, with the notable downregulation of CSFR-1 and TYRO-3.

In order to connect expression data to functional outcomes, we also assessed the expression of the cognate ligands of considered RTK. Interestingly, VEGF-A, FGF2 (a prototypical, but not the only, ligand for FGFRs) and IGF-1 were actually downregulated (vs naive samples) and ANG-1 (the Tie-2 ligand) was unchanged, suggesting that the upregulation of the mRNA for their receptor may not correspond to actual RTK engagement. On the other hand, Neuregulin-1 (a ligand for ErbB family, in particular ErbB4), HGF (ligand of HGFR/Met) and EphB3 were significantly upregulated (Fig. 2E), supporting the functional engagement of EGFR/ErbB4 and Met, respectively.

Thus, the targeted expression study reveals the induction of multiple RTKs and their ligands in correspondence of astrocytic, vascular and neuroimmune activation in pMICB.

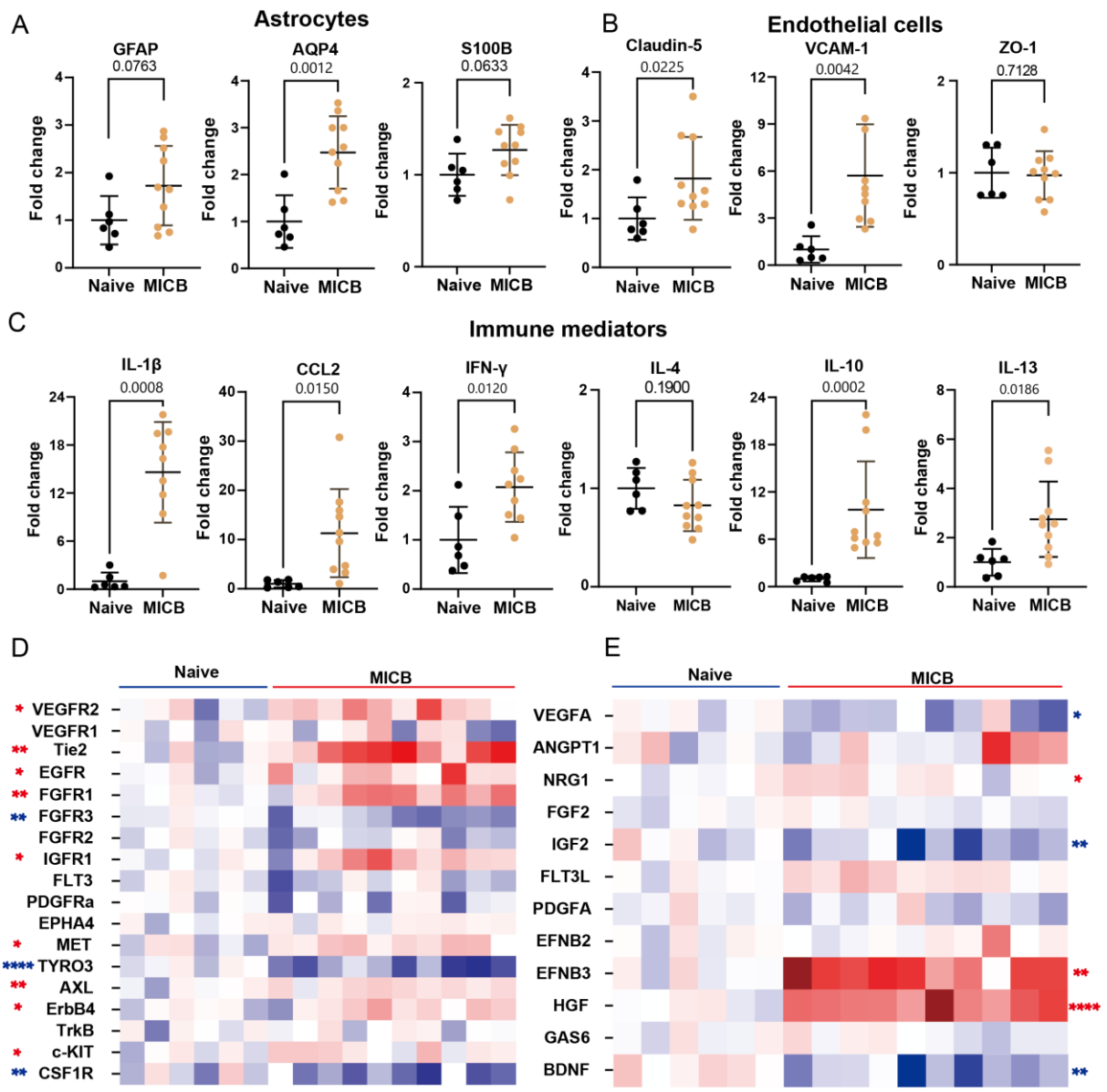

Figure 2. Expression survey of cortical tissue from the pMICB reveals astrocyte, vascular and immune activation. Sampling was performed at sacrifice, 36-48h after MICB induction. A. Expression of the astrocyte marker genes GFAP, AQP4 and S100β is upregulated to different extent in MICB samples. B. Expression of the endothelial markers Claudin-5 and VCAM-1 is upregulated in MICB, whereas expression of ZO-1 is unchanged. C. Expression of the pro-inflammatory genes IL-1β, CCL and IFN-γ is strongly upregulated in MICB. D. Expression of anti-inflammatory cytokines IL-10 and IL-13 is upregulated in MICB, whereas IL-4 expression is unaffected. E. Screening of the expression of a subset of RTK with high translational potential: compared to naive samples, MICB samples display the upregulation of VEGFR2, Tie-2, EGFR, FGFR1, IGFR1, EPHA4, MET, AXL, ErbB4 and the downregulation of CSF1R and TYRO-3. E. Expression screening for RTK ligands: NRG1, IGF-2, EFNB2 and HGF were significantly upregulated, whereas VEGF-A, FGF-2 and BDNF

were significantly downregulated. naive animals n=6, MICB animals n=10, * $p < 0.05$, ** $p < 0.01$, $p < 0.001$

ICP correlates with EGFR expression and astrocytes reactivity in the pMICB.

We investigated the molecular counterparts of ICH in the pMICB by performing a hierarchical cross-correlation clustering of a dataset, which included gene expression data and physiological parameters ICP and CPP. The k-means statistics (Fig. S1A) supported the identification of 7 distinct clusters (Fig.3A).

Notably, ICP clustered together with a set of 16 genes that included four RTKs (EGFR, Tyro3, TrkB and VEGFR1) and three RTK ligands (VEGFA, PDGFB, BDNF) together with MMP9, HIF1a, CD68, CCL2, GFAP and TIMP1. Interestingly, CPP did not cluster with ICP but rather in a separate group that included TNF-α and cKit. Five more clusters were identified: cluster 2 included IL-13 and TGF-α, cluster 3 included IGF-2, Neuregulin-1 and FGF2 together with FGFR3, cluster 4 included IL-33, IFN-γ and CCL-5, cluster 6 included HGF and MET, with ICAM1 and VCAM1, and cluster 7 included FGFR2, Tie2, FGFR1 and PDGFRa. The occurrence of discrete gene cluster sets indicates the co-induction of multiple transcriptional programs in the pMICB, but only one of these appears to be directly linked to ICP, either as cause or as possible consequence (i.e., HIF-1a upregulation corresponds to the hypoxia upon ICH).

We sought to obtain cellular context for the set of genes clustering with ICP in cluster 1 by performing a cell type deconvolution using data from the Allen Brain Atlas [37] (Fig 3B) (see methods). This analysis revealed that the majority of the genes in cluster 1 were strongly enriched in astrocytes, with secondary enrichment in microglia and, to a lesser extent, endothelial cells. Beside their co-expression in astrocytes, we sought an independent verification of the functional link between the astrocytic gene set correlated with ICP (namely GFAP, EGFR, TIMP1, CCL2, and BDNF; all with an enrichment score greater than 4). We performed a protein interaction analysis, which showed a strong co-expression pattern, indicative of functional links between the proteins (Fig 3C). Given the complex interplay of multiple astrocyte-related pathways in cluster 1 (EGFR, VEGFR1, PDGFA, PDGFB), we performed a STRING analysis to determine the central hub of the cluster that could serve as a key node linking all other targets. The STRING analysis identified EGFR as the most central gene, exhibiting the highest degree of centrality (0.81), suggesting a pivotal role in the ICP response (Fig S1B).

The gene expression data points toward the involvement of astrocyte responses triggered by EGFR in the pathophysiology of ICH. To further explore this model, we considered the correlation of EGFR expression either from the injury side or from the controlateral side with ICP and outcome, i.e., neurological evaluation and survival (Fig. S2A) across the animals in the experimental cohort. In fact, EGFR gene expression in the injury site displayed a strong trend toward direct correlation with Survival and mGCS (Fig S2B).

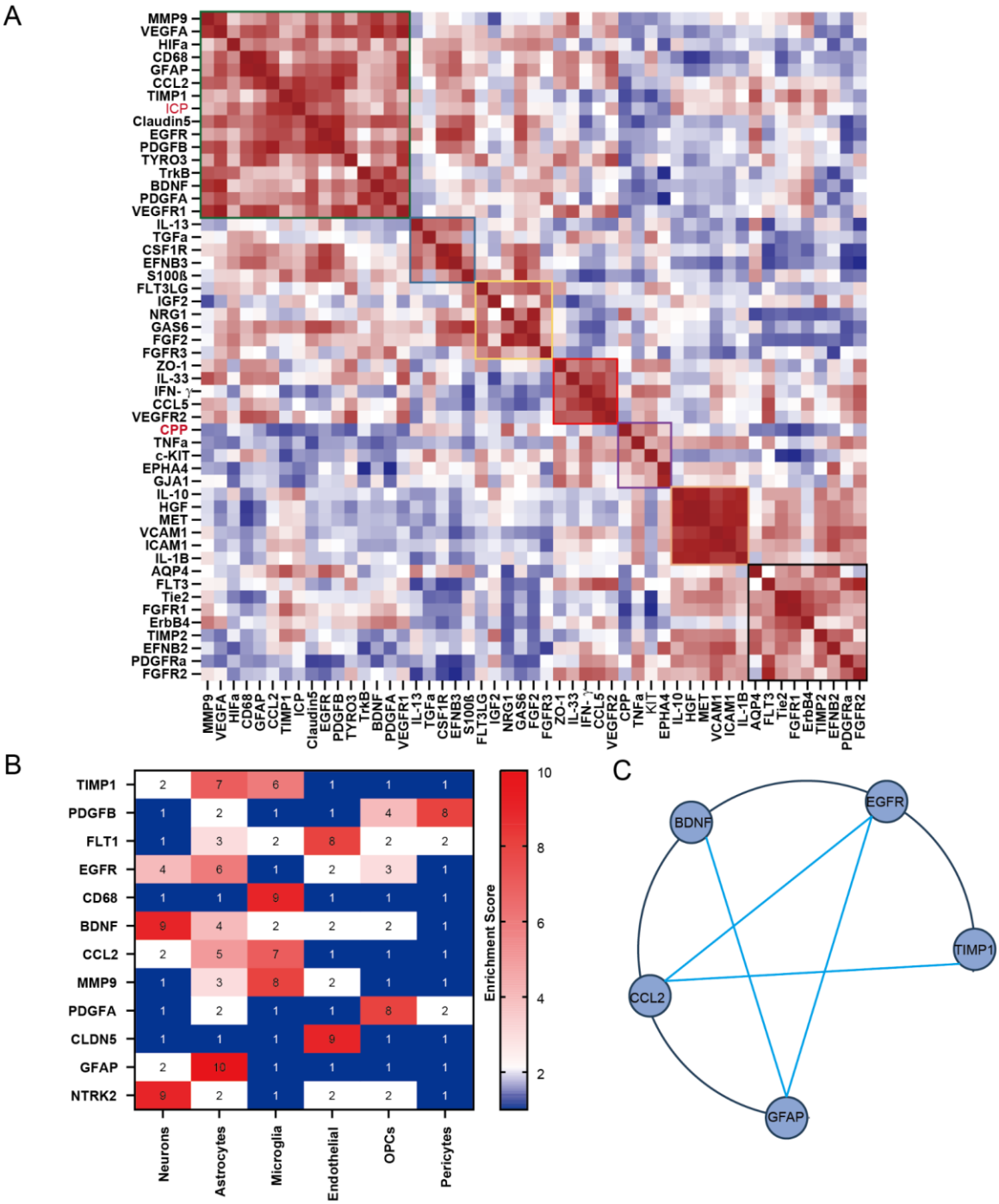

Figure 3. Intracranial pressure clusters with EGFR, VEGFR1 and astrocyte genes. A. Data from gene expression and from ICP and CPP measurement were integrated and subjected to unsupervised cross-correlation and clustering. Seven clusters were identified as the optimal configuration; cluster 1 includes ICP (in red) and several genes including EGFR, the hypoxia-factor HIF-1α and VEGFR1. CPP did not cluster with ICP but rather with TNF-α. Clusters 2 to 7 contain multiple cytokines and inflammatory mediators as well as their receptors. B. Cellular deconvolution of the genes clustering with ICP (cluster 1) in panel A reveals the enrichment in astrocyte genes, with smaller components of microglial and endothelial cells, indicating the relationship between ICP and astrocytes reactions to injury. C. STRING analysis confirms the direct interaction of the five most astrocyte-enriched genes identified by cellular deconvolution.

EGFR phosphorylation in the pMICB.

Although EGFR gene expression displays a trend toward correlation with ICP, EGFR mRNA levels alone may not fully capture the extent of EGFR engagement, signaling and turnover [38]. Therefore, we further explored the association between EGFR and ICP in the porcine MICB model by assessing the level of EGFR protein and the fraction of phosphorylation. As quality control, first we determined that tissue samples from the injured hemisphere displayed a robust increase in ERK phosphorylation (Fig. 4A-B). Interestingly, in whole-cortex protein extracts, levels of EGFR were reduced in injured compared to naive samples (Fig. 4C-D) but the total quantity of phosphorylated EGFR was comparable, indicating a strong increase in the fraction of phosphorylated EGFR upon injury (Fig. 4C,4E). On the other hand, the total level and the phosphorylation fraction for VEGFR2 (Fig. 4F,4I,4J) was decreased (and unmodified for Tie-2 (Fig. 4F,4G,4H)), implying the downregulation of the signaling through this receptor.

Furthermore, we reasoned that increased phosphorylation fraction for EGFR may correspond to the increased engagement by its ligands; whereas the opposite may be true for RTK whose phosphorylation is downregulated. Thus, we verified the protein levels of the ligand partners of the three RTK under study: among EGFR ligands, EGF and Neuregulin 1 levels were significantly increased (Fig4. K-M) but not those of TGF-α (Fig. 4N). Conversely, VEGF-A protein levels were downregulated compared to naive samples, and Tie-2 binding ANG-1 was not altered (Fig. 4O-P). Thus, increased EGFR phosphorylation was matched by the upregulation of at least two of its ligands, whereas the opposite was true for VEGFR2.

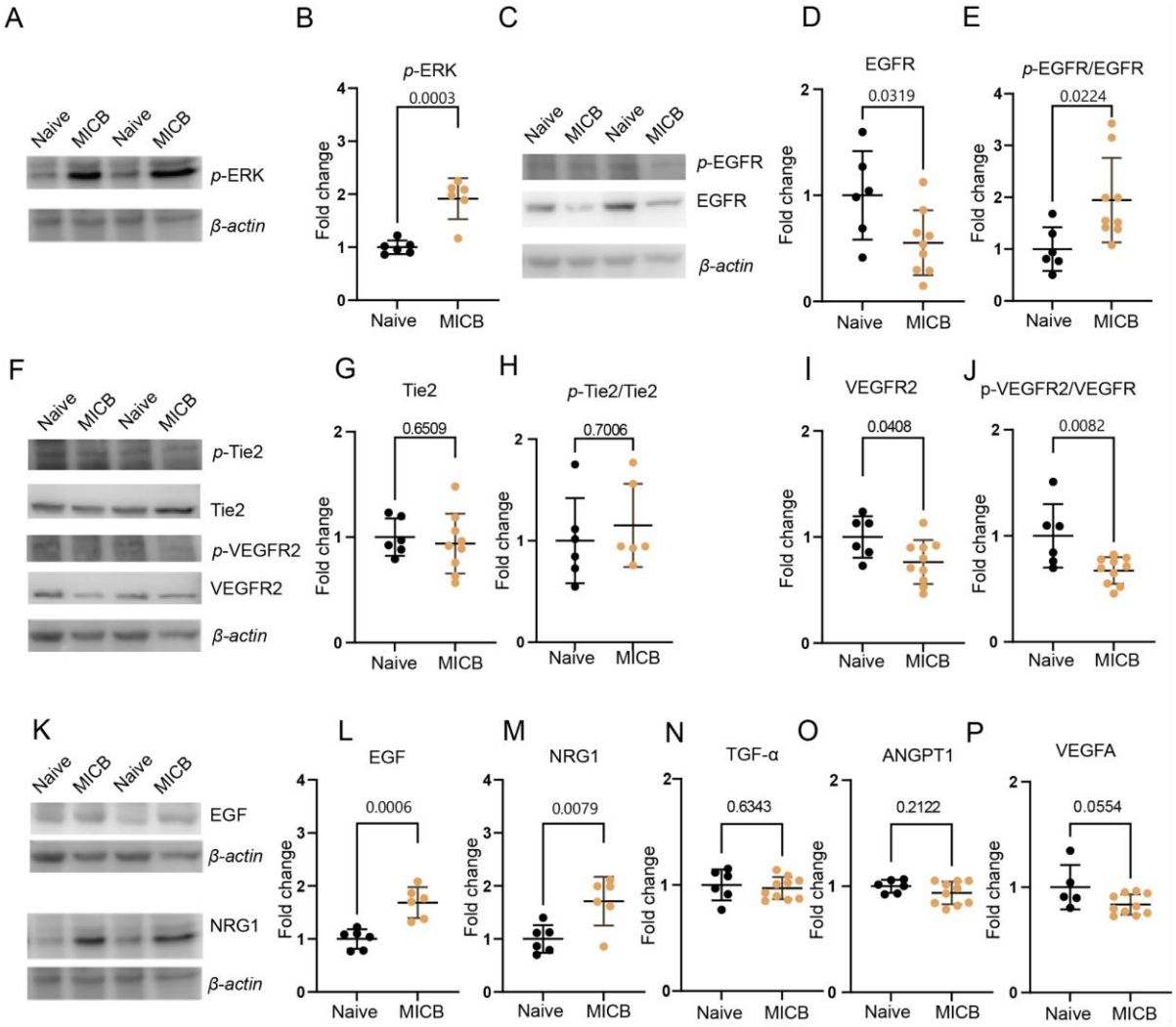

Figure 4. EGF upregulation and EGFR phosphorylation in MICB. A-B. Whole-tissue Western Blot (WB) reveals the Increased phosphorylation of ERK1/2 in MICB samples compared to naive. C-E Increased phosphorylation ratio of the EGFR despite the decrease of total EGFR in MICB samples revealed by whole-tissue WB. F-H. Unmodified levels of total or phosphorylated Tie-2 in MICB samples. I-J. Decrease in the phosphorylation of VEGFR2, with decreased total VEGFR2 protein levels. K-N WB for EGFR family ligands shows an increase in EGF protein and Neuregulin-1 and unchanged TGF-α in MICB whole-tissue protein extracts probed by WB. O.ANGPT1 protein levels in MICB whole-tissue protein extracts probed by nitrocellulose antibody array. P. Strong trend toward decrease protein level of VEGF-A in MICB protein extracts probed by glass antibody array. Naive n=6, MICB n=10.

EGFR activation results in reactive astrocytosis and poor outcome

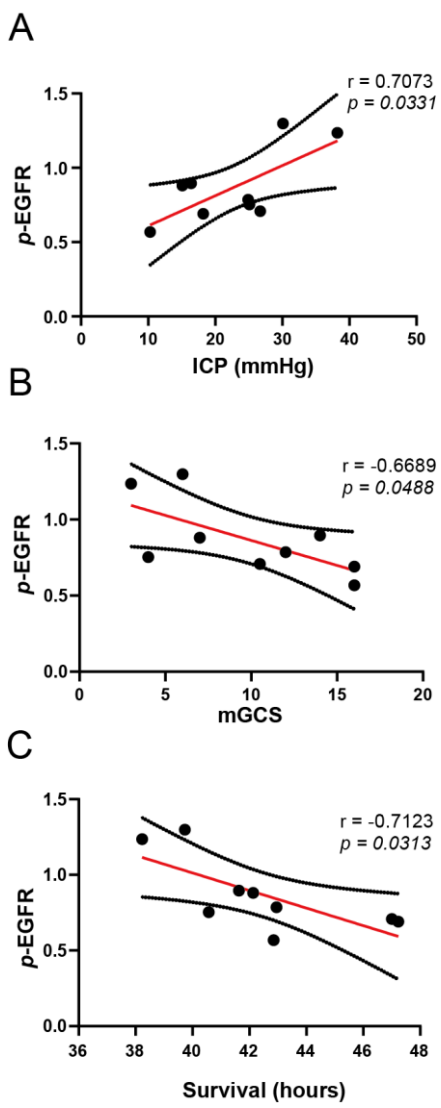

Finally, we sought to verify the clinical impact of EGFR activation in the pMICB tissue samples..

To verify this, we correlated the fraction of phospho-EGFR within the ipsilateral side ICP, Survival (time from injury) and modified GCS measured at the termination. Most notably, pEGFR was strongly and significantly correlated directly with ICP (r=0.7073 ; p= 0.0331 over an ICP range 10-40 mmHg). Moreover, phospho-EGFR was inversely correlated with survival, with higher levels of EGFR corresponding to shorter survival (r=-0.7123 ; p= 0.031) and to deeper coma (inverse correlation to mGCS, r= -0.6689 ; p= 0.0488). No correlation was detected between pVEGFR2 or p-Tie2 levels and clinico-physiological parameters.

Taken together, this data show that the EGFR cascade is active in pMICB samples and correlated with ICP multiple outcome measures.

Figure 5. EGFR phosphorylation correlates with ICP and survival. A. The fraction of phosphorylated EGFR determined by WB in whole-tissue protein extract directly correlates with ICP measured at the end of the follow-up of each animal. B. The fraction of phosphorylated EGFR is inversely correlated with neurological involvement determined by the modified porcine Glasgow Coma Scale. C. The fraction of phosphorylated EGFR inversely correlates with survival of the animals, determined as the time-point in which termination criteria are reached.

Discussion

In the present work we show that increased ICP in a pig MICB model is directly related to vascular, astrocytic and inflammatory transcriptional signatures as well as with the transcriptional modulation of a discrete set of RTK including EGFR, VEGFR2, FGFR and Tie-2. In particular, mRNA levels and phosphorylation of the EGF receptor, but not of the VEGFR or Tie-2, correlates on one side with astrocytes reactivity and on the other side with ICP, animal survival and depth of coma, so that increased EGFR transcription and activation correspond to increased ICP and reduced survival. Thus, EGFR appears to be strongly involved in brain edema and ICH in the post-acute (36-48h) window.

Our data point toward a complex set of transcriptional changes affecting RTKs in cortex upon cerebral injury, potentially related to the multiple co-occurring biological responses to traumatic or vascular injury[39]. These findings are largely, but not completely, in agreement with the patterns of RTK phosphorylation observed in murine models of TBI (e.g, EGFR/Erb and Met activation;[18,19,40], suggesting some degree of evolutionary convergence in the brain injury response. Among the divergent effects, VEGFR2 and Tie-2 phosphorylation appears to be already downregulated in the pMICB at 2dpi compared to the mTBI (where they are still upregulated at 3dpi or 7dpi). Thus, VEGFR2 does not appear to have a prominent relationship to intracranial pressure at this stage of the pMICB model, in contrast to what shown in other neoplastic or vascular diseases[41,42], this unexpected finding may be possibly indicating a faster resolution of the vascular permeability disruption in the porcine model. Importantly, the role of neurointensive care should also be considered: whereas most murine TBI models lack standard hemodynamic, respiratory and/or metabolic support measures, the porcine model benefits from comprehensive intensive care management, which could itself facilitate a more rapid recovery. As such, differences between species may not be solely evolutionary but also reflect the greater clinical complexity of the large animal model. This point is highly relevant to translational research, as human patients likewise receive intensive medical support—something that is typically absent in mouse studies. This mismatch between model systems has often been cited as a major factor contributing to the poor translational success of rodent TBI data [43], highlighting the need for more clinically realistic preclinical models [44].

Interestingly, EGFR appears to be highly correlated with ICP and other physiological readouts, as well as highly correlated with several reactive-astrocyte markers (such as GFAP, TIMP1 and TIMP2) but also, surprisingly, to neuroinflammatory mediators such as CCL2 and MMP9. These findings well agree with the concept of EGFR driving the transition between homeostatic and reparative astrocytic states[34]: EGFR is a major inducer of astrocytes proliferation[45] necessary to astrocytic scar formation[46] but also appears to control two

additional sets of response to injury, namely inflammation and water/ion fluxes, which may relate to the onset of brain edema and ICH. In fact, EGFR upregulation is associated with CCL2 expression in astrocytes upon pMCIB, possibly stimulating the influx of macrophages and immune cells (hence, their co-clustering with MMP9 and CD68; Fig. 3A). A similar induction of CCL2 by EGFR family members has been previously reported in mutant-EGFR-driven gliomas, where the extent of K-Ras activation by EGFR correlates with CCL2 induction and macrophage infiltration[47] and reduced availability of EGFR ligands suppresses CCL2[48]. Moreover, there is evidence that EGFR signaling may contribute to microglial inflammation in spinal cord injury models[49].

EGFR activation may compromise the astrocyte-dependent water flux and contribute to astrocytes swelling. Aquaporins (AQP) are the main water transport channels in mammalian cells and AQP4 is the main astrocytic AQP, highly enriched on astrocitic end-feet[50]. Interestingly, whereas AQP4 knock-out reduces cytotoxic edema by reducing water influx during cellular injury, loss of AQP4 may worsen VBE by limiting the removal of inflown water [51]. EGFR appears to prevent the insertion of some AQPs (such as AQP2[52]) and there is an inverse correlation of EGFR and AQP4 expression in cultured astrocytes[53]. Although the molecular details linking EGFR to AQP4 in astrocytes are still lacking, one may speculate, on the base on the available evidence, that EGFR may reduce AQP4 availability in astrocytes and therefore impair the water outflow and maintain the increased ICP due to the VBE. Additional mechanisms linking EGFR to ICP through astrocytes may include the increase in cellular volume[34], the induction of metalloproteases[54] and the disregulation of ion channel expressions on astrocytes[9].

Intriguingly, despite the robust EGFR activation, EGF itself is not expressed in brain parenchyma in pMICB although it is present there at protein level in substantial quantities upon injury (see Fig. 4E); on the other hand, TGF-α (enriched in astrocytes themselves as well as in neurons[55]) appears not to be altered. Conversely, the ErbB4-selective ligand Neuregulin-1 is upregulated. Thus, it is conceivable that the EGFR signaling is not triggered by the endogenous upregulation of EGF (or other EGFR ligands), but rather it is driven by exogenous EGF, e.g. derived from blood products in the CSF [56]. In such a scenario, EGF may act as an additional Damage-Associated Molecular Pattern to kick-start the CNS response to injury.

Notably, EGFR upregulation activation is not unique to pMCIB, but it has been reported in several brain and spinal cord injury models, as part of a fundamental astrocytes response to injury[34,57].

In several settings, however, acute inhibition of EGFR was beneficial: Lapatinib improved motor performance after TBI[40] and blockade of EGFR also limited secondary damage in spinal cord injury [49,58,59] although note the lack of effect reported by Sharp et al., 2012[60]. On the other hand, EGFR may be necessary to the formation of the astrocytic scar, and therefore short-term, but not long-term, EGFR suppression may be beneficial.

The present study is not without limitations: first, the present MICB is not a model of intracranial bleeding, whose brain edema pathophysiology may be only partially overlapping the one unfolding in TBI and, therefore, the comparison between pMICB and TBI should be performed with caution. To this respect, it is necessary to note that the extent of compression and hypoxia may differ in different types of trauma, with differential involvement of RTKs subfamilies. Second, the present study was not designed to directly address the causal link between increased ICP and EGFR phosphorylation, and a dedicated study involving one or more EGFR inhibitors, administered within the acute phase window, is necessary to investigate such link. Third, EGFR is a prominent but not the only one of several RTK phosphorylated upon MICB, and a more effective treatment strategy may need the engagement of multiple targets, i.e., with RTK inhibitors endowed with broad selectivity.

In conclusion, we provide evidence linking EGFR signaling to intracranial hypertension and outcome in a porcine MICB, suggesting that EGFR may control astrocytes reactivity and contribute to the unresolved VBE (Fig.6). Thus, short-term EGFR inhibitors may reduce ICP in acute brain injury settings.

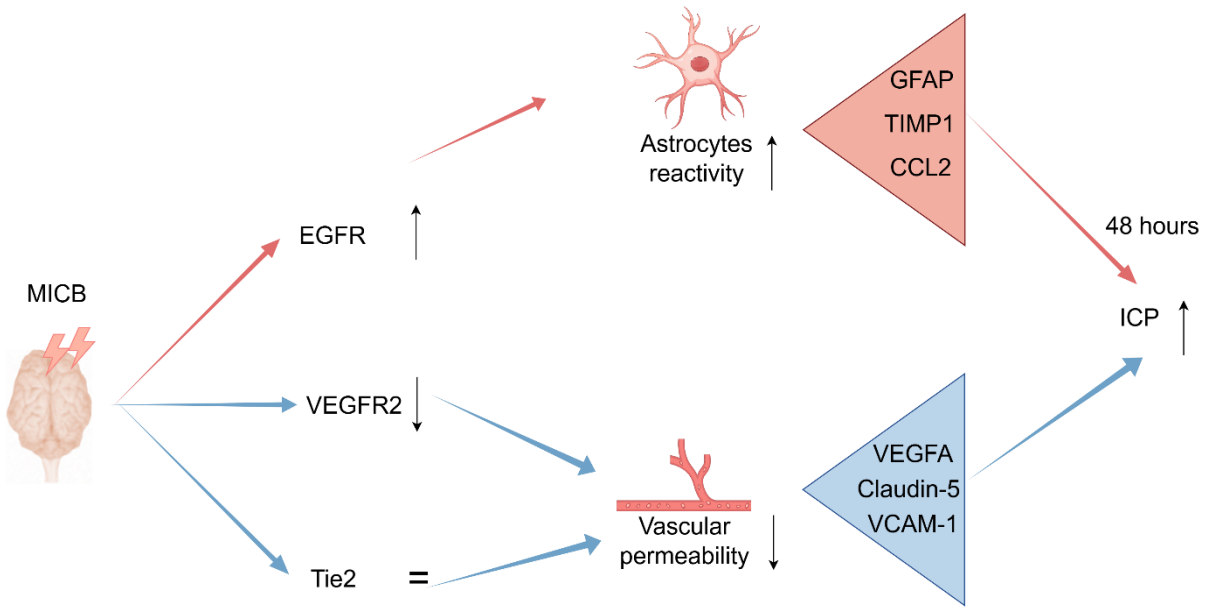

Figure 6. Concluding cartoon

Acknowledgement

We sincerely thank Thomas Lenk and Florian olde Huevel (Department of Neurology, Ulm University) for technical and experimental support.

Fundings

This work is funded by the Deutsche Forschungsgemeinschaft (DFG, German Research Foundation)– Project-ID 251293561 – SFB 1149. Z.Z is supported by the China Scholarship Council (Personal certificate No.202308320129).

Authors´contributions

Conceptualization. F.R., M.P., T.K., P.R.; data curation Z.Z M.P.; formal analysis F.R., Z.Z., M.P.; funding acquisition and investigation F.R., P.R.; methodology A.H., Z.Z., F.S., T.M., B.O., M.G., S.K., E.C., F.M., M.P., P.R.; supervision F.R., M.P., T.K., P.R.; writing—original draft M.P., F.R., P.R.; writing—review & editing F.R., P.R., T.K., M.P.; all authors have read and agreed to the published version of the manuscript.

References

1. Stocchetti N, Maas AI. Traumatic intracranial hypertension. The New England journal of medicine 2014;370(22):2121-30, doi:10.1056/NEJMra1208708
2. Wan Y, Holste KG, Hua Y, et al. Brain edema formation and therapy after intracerebral hemorrhage. Neurobiology of disease 2023;176(105948, doi:10.1016/j.nbd.2022.105948
3. Gao G, Wu X, Feng J, et al. Clinical characteristics and outcomes in patients with traumatic brain injury in China: a prospective, multicentre, longitudinal, observational study. The Lancet Neurology 2020;19(8):670-677, doi:10.1016/s1474-4422(20)30182-4
4. Kevci R, Hånell A, Howells T, et al. Temporal dynamics of ICP, CPP, PRx, and CPPopt in relation to outcome in spontaneous intracerebral hemorrhage. Journal of neurosurgery 2025;1-11, doi:10.3171/2024.10.jns241038
5. Carney N, Totten AM, O'Reilly C, et al. Guidelines for the Management of Severe Traumatic Brain Injury, Fourth Edition. Neurosurgery 2017;80(1):6-15, doi:10.1227/neu.0000000000001432
6. Codorniu A, Charbit E, Werner M, et al. Comparison of mannitol and hypertonic saline solution for the treatment of suspected brain herniation during prehospital management of traumatic brain injury patients. European journal of emergency medicine : official journal of the European Society for Emergency Medicine 2024;31(4):287-293, doi:10.1097/mej.0000000000001138
7. Gaither JB, Spaite DW, Bobrow BJ, et al. EMS Treatment Guidelines in Major Traumatic Brain Injury With Positive Pressure Ventilation. JAMA surgery 2024;159(4):363-372, doi:10.1001/jamasurg.2023.7155
8. Hawryluk GWJ, Rubiano AM, Totten AM, et al. Guidelines for the Management of Severe Traumatic Brain Injury: 2020 Update of the Decompressive Craniectomy Recommendations. Neurosurgery 2020;87(3):427-434, doi:10.1093/neuros/nyaa278
9. Jha RM, Kochanek PM, Simard JM. Pathophysiology and treatment of cerebral edema in traumatic brain injury. Neuropharmacology 2019;145(Pt B):230-246, doi:10.1016/j.neuropharm.2018.08.004

10. Stokum JA, Shim B, Negoita S. Cation flux through SUR1-TRPM4 and NCX1 in astrocyte endfeet induces water influx through AQP4 and brain swelling after ischemic stroke. 2023;16(788):eadd6364, doi:10.1126/scisignal.add6364
11. Mestre H, Du T. Cerebrospinal fluid influx drives acute ischemic tissue swelling. 2020;367(6483), doi:10.1126/science.aax7171
12. Yang C, Hawkins KE, Doré S, et al. Neuroinflammatory mechanisms of blood-brain barrier damage in ischemic stroke. 2019;316(2):C135-c153, doi:10.1152/ajpcell.00136.2018
13. Wu M, Gong Y, Jiang L, et al. VEGF regulates the blood-brain barrier through MMP-9 in a rat model of traumatic brain injury. Experimental and therapeutic medicine 2022;24(6):728, doi:10.3892/etm.2022.11664
14. Krueger M, Mages B, Hobusch C, et al. Endothelial edema precedes blood-brain barrier breakdown in early time points after experimental focal cerebral ischemia. Acta neuropathologica communications 2019;7(1):17, doi:10.1186/s40478-019-0671-0
15. Jeon H, Kim M, Park W, et al. Upregulation of AQP4 Improves Blood-Brain Barrier Integrity and Perihematomal Edema Following Intracerebral Hemorrhage. 2021;18(4):2692-2706, doi:10.1007/s13311-021-01126-2
16. Easton AS. Regulation of permeability across the blood-brain barrier. Advances in experimental medicine and biology 2012;763(1-19, doi:10.1007/978-1-4614-4711-5_1
17. DiNuzzo M, Mangia S, Maraviglia B, et al. Regulatory mechanisms for glycogenolysis and K+ uptake in brain astrocytes. Neurochemistry international 2013;63(5):458-64, doi:10.1016/j.neuint.2013.08.004
18. Rehman R, Miller M, Krishnamurthy SS, et al. Met/HGFR triggers detrimental reactive microglia in TBI. Cell reports 2022;41(13):111867, doi:10.1016/j.celrep.2022.111867
19. Rehman R, Froehlich A, Olde Heuvel F, et al. The FGFR inhibitor Rogaratinib reduces microglia reactivity and synaptic loss in TBI. Frontiers in immunology 2024;15(1443940, doi:10.3389/fimmu.2024.1443940
20. Saraon P, Pathmanathan S, Snider J, et al. Receptor tyrosine kinases and cancer: oncogenic mechanisms and therapeutic approaches. 2021;40(24):4079-4093, doi:10.1038/s41388-021-01841-2
21. Kapapa T, Wernheimer V, Hoffmann A, et al. Unravelling Secondary Brain Injury: Insights from a Human-Sized Porcine Model of Acute Subdural Haematoma. 2024;14(1), doi:10.3390/cells14010017
22. Datzmann T, Münz F, Hoffmann A, et al. An exploratory study investigating the effect of targeted hyperoxemia in a randomized controlled trial in a long-term resuscitated model of combined acute subdural hematoma and hemorrhagic shock in cardiovascular healthy pigs. Frontiers in immunology 2023;14(1123196, doi:10.3389/fimmu.2023.1123196
23. Datzmann T, Messerer DAC, Münz F, et al. The effect of targeted hyperoxemia in a randomized controlled trial employing a long-term resuscitated, model of combined acute subdural hematoma and hemorrhagic shock in swine with coronary artery disease: An exploratory, hypothesis-generating study. Frontiers in medicine 2022;9(971882, doi:10.3389/fmed.2022.971882
24. Datzmann T, Kapapa T, Scheuerle A, et al. In-depth characterization of a long-term, resuscitated model of acute subdural hematoma-induced brain injury. Journal of neurosurgery 2021;134(1):223-234, doi:10.3171/2019.9.jns191789
25. Pedregosa F, Varoquaux G, Gramfort A, et al. Scikit-learn: Machine Learning in Python. Journal of Machine Learning Research 2011;
26. Hunter JD. Matplotlib: A 2D Graphics Environment. Computing in Science & Engineering 2007;9(3):90-95, doi:10.1109/MCSE.2007.55
27. Yao Z, van Velthoven CTJ, Nguyen TN, et al. A taxonomy of transcriptomic cell types across the isocortex and hippocampal formation. Cell 2021;184(12):3222-3241.e26, doi:10.1016/j.cell.2021.04.021
28. Virshup I, Bredikhin D, Heumos L, et al. The scverse project provides a computational ecosystem for single-cell omics data analysis. Nature Biotechnology 2023;41(5):604-606, doi:10.1038/s41587-023-01733-8

29. Szklarczyk D, Kirsch R, Koutrouli M. The STRING database in 2023: protein-protein association networks and functional enrichment analyses for any sequenced genome of interest. 2023;51(D1):D638-d646, doi:10.1093/nar/gkac1000
30. Shannon P, Markiel A, Ozier O, et al. Cytoscape: a software environment for integrated models of biomolecular interaction networks. Genome research 2003;13(11):2498-504, doi:10.1101/gr.1239303
31. Hu Y, Zheng Y, Wang T, et al. VEGF, a Key Factor for Blood Brain Barrier Injury After Cerebral Ischemic Stroke. Aging and disease 2022;13(3):647-654, doi:10.14336/ad.2021.1121
32. Wang LF, Li X, Gao YB, et al. Activation of VEGF/Flk-1-ERK Pathway Induced Blood-Brain Barrier Injury After Microwave Exposure. Molecular neurobiology 2015;52(1):478-91, doi:10.1007/s12035-014-8848-9
33. Fang Z, He QW, Li Q, et al. MicroRNA-150 regulates blood-brain barrier permeability via Tie-2 after permanent middle cerebral artery occlusion in rats. FASEB journal : official publication of the Federation of American Societies for Experimental Biology 2016;30(6):2097-107, doi:10.1096/fj.201500126
34. Liu B, Chen H, Johns TG, et al. Epidermal growth factor receptor activation: an upstream signal for transition of quiescent astrocytes into reactive astrocytes after neural injury. The Journal of neuroscience : the official journal of the Society for Neuroscience 2006;26(28):7532-40, doi:10.1523/jneurosci.1004-06.2006
35. Luo J, Miller MW. Platelet-derived growth factor-mediated signal transduction underlying astrocyte proliferation: site of ethanol action. The Journal of neuroscience : the official journal of the Society for Neuroscience 1999;19(22):10014-25, doi:10.1523/jneurosci.19-22-10014.1999
36. Huang Y, Happonen KE, Burrola PG, et al. Microglia use TAM receptors to detect and engulf amyloid β plaques. 2021;22(5):586-594, doi:10.1038/s41590-021-00913-5
37. Lein ES, Hawrylycz MJ, Ao N, et al. Genome-wide atlas of gene expression in the adult mouse brain. Nature 2007;445(7124):168-76, doi:10.1038/nature05453
38. Conte A, Sigismund S. Chapter Six - The Ubiquitin Network in the Control of EGFR Endocytosis and Signaling. Progress in molecular biology and translational science 2016;141(225-76, doi:10.1016/bs.pmbts.2016.03.002
39. Morganti-Kossmann MC, Semple BD, Hellewell SC, et al. The complexity of neuroinflammation consequent to traumatic brain injury: from research evidence to potential treatments. Acta neuropathologica 2019;137(5):731-755, doi:10.1007/s00401-018-1944-6
40. Chandrasekar A, Olde Heuvel F, Wepler M, et al. The Neuroprotective Effect of Ethanol Intoxication in Traumatic Brain Injury Is Associated with the Suppression of ErbB Signaling in Parvalbumin-Positive Interneurons. Journal of neurotrauma 2018;35(22):2718-2735, doi:10.1089/neu.2017.5270
41. Gerstner ER, Duda DG, di Tomaso E, et al. VEGF inhibitors in the treatment of cerebral edema in patients with brain cancer. Nature reviews Clinical oncology 2009;6(4):229-36, doi:10.1038/nrclinonc.2009.14
42. Kim E, Yang J, Park KW, et al. Inhibition of VEGF Signaling Reduces Diabetes-Exacerbated Brain Swelling, but Not Infarct Size, in Large Cerebral Infarction in Mice. Translational stroke research 2018;9(5):540-548, doi:10.1007/s12975-017-0601-z
43. Nyanzu M, Siaw-Debrah F, Ni H, et al. Improving on Laboratory Traumatic Brain Injury Models to Achieve Better Results. International journal of medical sciences 2017;14(5):494-505, doi:10.7150/ijms.18075
44. O'Donnell JC, Browne KD. Multimodal Neuromonitoring and Neurocritical Care in Swine to Enhance Translational Relevance in Brain Trauma Research. 2023;11(5), doi:10.3390/biomedicines11051336
45. Aldape K, Zadeh G, Mansouri S, et al. Glioblastoma: pathology, molecular mechanisms and markers. Acta neuropathologica 2015;129(6):829-48, doi:10.1007/s00401-015-1432-1

46. Lin HW, Basu A, Druckman C, et al. Astrogliosis is delayed in type 1 interleukin-1 receptor-null mice following a penetrating brain injury. Journal of neuroinflammation 2006;3(15, doi:10.1186/1742-2094-3-15
47. An Z, Knobbe-Thomsen CB, Wan X, et al. EGFR Cooperates with EGFRvIII to Recruit Macrophages in Glioblastoma. Cancer research 2018;78(24):6785-6794, doi:10.1158/0008-5472.can-17-3551
48. Liu X, Huang Y, Qi Y, et al. The GBM Tumor Microenvironment as a Modulator of Therapy Response: ADAM8 Causes Tumor Infiltration of Tams through HB-EGF/EGFR-Mediated CCL2 Expression and Overcomes TMZ Chemosensitization in Glioblastoma. 2022;14(19), doi:10.3390/cancers14194910
49. Qu WS, Tian DS, Guo ZB, et al. Inhibition of EGFR/MAPK signaling reduces microglial inflammatory response and the associated secondary damage in rats after spinal cord injury. Journal of neuroinflammation 2012;9(178, doi:10.1186/1742-2094-9-178
50. Rash JE, Yasumura T, Hudson CS, et al. Direct immunogold labeling of aquaporin-4 in square arrays of astrocyte and ependymocyte plasma membranes in rat brain and spinal cord. Proceedings of the National Academy of Sciences of the United States of America 1998;95(20):11981-6, doi:10.1073/pnas.95.20.11981
51. Li Y, Wang Y, Huang X, et al. Role of aquaporins in brain water transport and edema. Frontiers in neuroscience 2025;19(1518967, doi:10.3389/fnins.2025.1518967
52. Babicz RSE, Baylor N, Terlouw A, et al. Ribosomal s6 kinase is a mediator of aquaporin-2 S256 phosphorylation and membrane accumulation after EGFR inhibition with erlotinib. 2025;328(3):F344-f359, doi:10.1152/ajprenal.00353.2024
53. Scholze AR, Foo LC, Mulinyawe S, et al. BMP Signaling in Astrocytes Downregulates EGFR to Modulate Survival and Maturation. PLOS ONE 2014;9(10):e110668, doi:10.1371/journal.pone.0110668
54. Chen XC, Wei XT, Guan JH, et al. EGF stimulates glioblastoma metastasis by induction of matrix metalloproteinase-9 in an EGFR-dependent mechanism. Oncotarget 2017;8(39):65969-65982, doi:10.18632/oncotarget.19622
55. Karki P, Johnson J, Jr., Son DS, et al. Transcriptional Regulation of Human Transforming Growth Factor-α in Astrocytes. Molecular neurobiology 2017;54(2):964-976, doi:10.1007/s12035-016-9705-9
56. Sirko S, Schichor C, Della Vecchia P, et al. Injury-specific factors in the cerebrospinal fluid regulate astrocyte plasticity in the human brain. Nature Medicine 2023;29(12):3149-3161, doi:10.1038/s41591-023-02644-6
57. Sun D, Bullock MR, Altememi N, et al. The effect of epidermal growth factor in the injured brain after trauma in rats. Journal of neurotrauma 2010;27(5):923-38, doi:10.1089/neu.2009.1209
58. Li ZW, Zhao JJ, Li SY, et al. Blocking the EGFR/p38/NF-κB signaling pathway alleviates disruption of BSCB and subsequent inflammation after spinal cord injury. Neurochemistry international 2021;150(105190, doi:10.1016/j.neuint.2021.105190
59. Erschbamer M, Pernold K, Olson L. Inhibiting epidermal growth factor receptor improves structural, locomotor, sensory, and bladder recovery from experimental spinal cord injury. The Journal of neuroscience : the official journal of the Society for Neuroscience 2007;27(24):6428-35, doi:10.1523/jneurosci.1037-07.2007
60. Sharp K, Yee KM, Steward O. A re-assessment of the effects of treatment with an epidermal growth factor receptor (EGFR) inhibitor on recovery of bladder and locomotor function following thoracic spinal cord injury in rats. Experimental neurology 2012;233(2):649-59, doi:10.1016/j.expneurol.2011.04.013